ORIGINAL PAPER

Characteristics of roof rock failure during coal seam mining and prediction techniques for mine water inflow in exposed karst areas

Bo Li[1] · Qiang Wu[2] · Yu Yang[1] · Huang Wu[1] · Tao Li[3]

Abstract

The failure characteristics of roof strata in coal mining and the accurate prediction of mine water inflow are prerequisites for mine safety. Taking a typical coal mine in Southwest China as a case, a new type of similar material suitable for coal mine in exposed karst areas was developed. Through the physical and numerical simulation, the failure characteristics of overlaying rock in karst areas were analyzed. The results showed that the plastic zone developed and accumulated from the roof. After mining, the stress and displacement of overlying rock were divided into three areas along the mining direction. The middle area experienced the maximum change. Overall, the height of falling and water-conducting fracture zones in karst exposed areas was slightly lower than that in other areas. And then, the hydrogeological structure considering the water-conducting fracture zone was rationally generalized, and a three-dimensional numerical model for predicting mine water inflow was built. It was found that the numerical simulation method had the minimum error and the maximum accuracy than other traditional methods, and its results were the closest to the measured value, which could more truly reflect the dynamic formation process of mine water inflow.

✉ Bo Li
  bli8@gzu.edu.cn

[1] Key Laboratory of Karst Georesources and Environment, Ministry of Education, Guizhou University, Guiyang 550025, China

[2] College of Earth Science and Surveying Engineering, China University of Mining and Technology (Beijing), Beijing 100083, China

[3] School of Mines and Civil Engineering, Liupanshui Normal University, Liupanshui 553004, China

Graphical Abstract
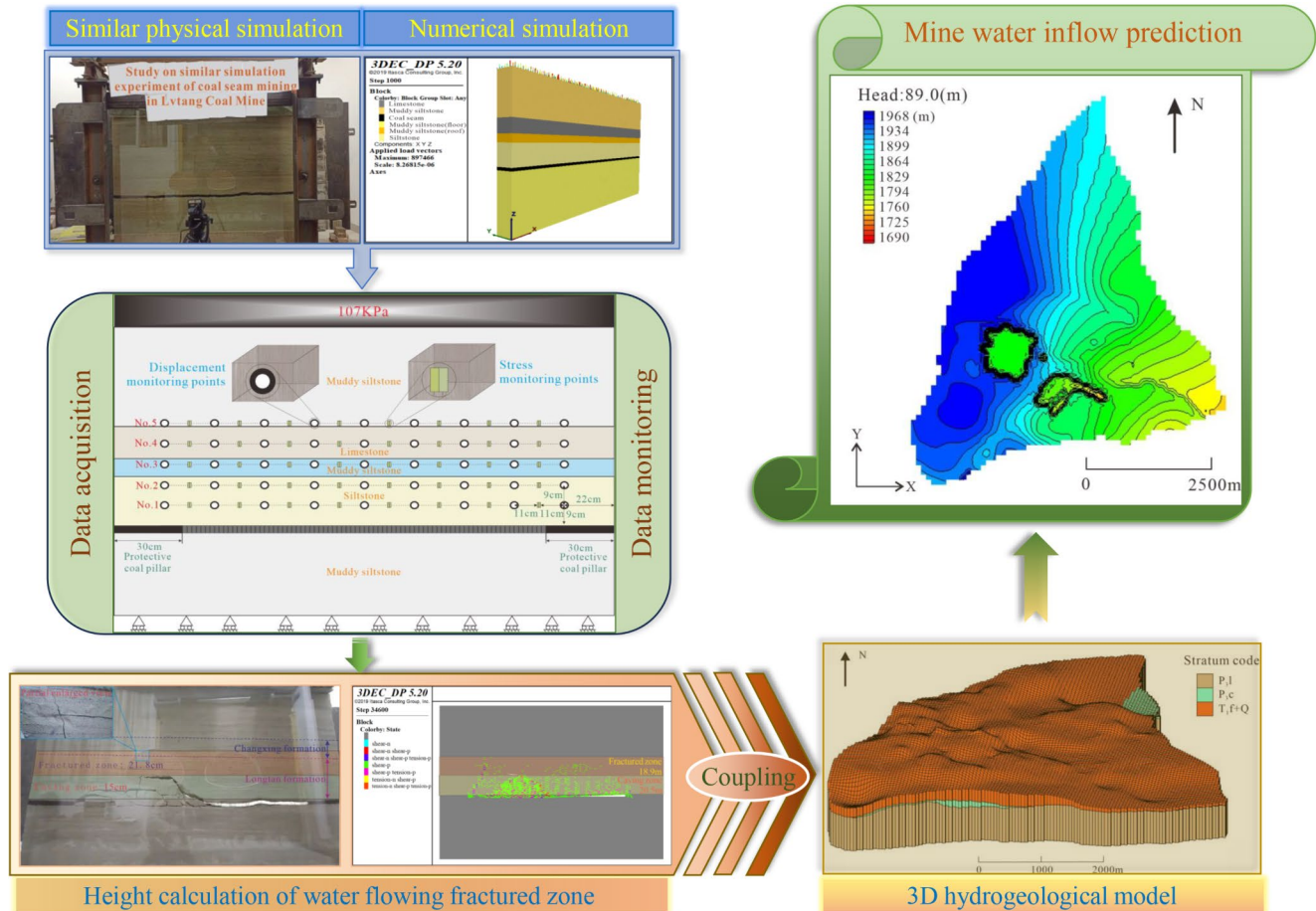
Introduction

Coal is an important basic energy source in the world, which provides an important energy guarantee for the development of global economy and society. The prediction of mine water inflow can provide a basis for mine design, mining planning and water disaster prevention and control, which is also of great significance during the entire life cycle of mines (Huang et al. 2016; Roy et al. 2020; Singh et al. 1985). Mine water inflow refers to the amount of water that enters the mine from various water sources through different channels during mine construction or production (Guo et al. 2009). Accurate prediction of mine water inflow has always been a key problem that endangers mine work safety. The existing mine water inflow prediction methods take the mining area and historical water inflow data as the main basis for predicting the mine water inflow, which does not accurately reflect the formation process of water inflow (Miao et

al. 2013). The part of mine inflow is recharged from the coal measure aquitard itself, and another part is recharged from adjacent aquifers in mining fracture zones (Wu et al. 2017). Water in the adjacent aquifers will enter the mine through the mining fracture zone. When it does not develop into the aquifer, water will not directly replenish to the mine. Therefore, when calculating the corresponding water inflow, the entire mining area cannot be taken as a water-conducting channel (Zeng et al. 2023). The mine water inflow should be calculated based on the fact that the mining fracture zone leading to the adjacent aquifer acts as a water-conducting channel, which is more in line with the formation mechanism of water inflow (Islam et al. 2016; Li et al. 2023; Ma et al. 2022). For mines that water source is mainly from the roof aquifer, it is first necessary to determine the height of falling zone and fracture zone formed in coal mining. During current study on overlaying rock failure in coal mining, the numerical and similar simulation methods are preferred

(Erguler and Ulusay 2009; Feng et al. 2014; Lawson et al. 2017; Poulsen et al. 2015; Zhao et al. 2018). For example, Zhu et al. (2008) conducted numerical simulation analysis on the coal mining process by using RFPA2D software, and identified the deformation and failure of roof strata and the characteristics of groundwater seepage. Yao et al. (2012) analyzed the changes in the stress, water pressure and seepage field of roof surrounding rock during coal mining by using RFPA2D and COMSOL software. Yanli et al. (2011) built a similar model about the overlying strata on the long-arm working face of coal mining by using sponge and plastic foam, and studied the deformation and failure characteristics of the overlying strata. Wei et al. (2022) studied the development of water-conducting fracture zones in the overlying bedrock during the mining of extremely thick coal seams with large buried depth through physical simulation tests. All these researches contributed to the study on failure mechanism of overlaying rock in coal mining, but their focus was put on sandstone or mudstone roofs. However, the lithology of coal roof in the exposed karst area is more complex, and the deformation and failure characteristics of the overlying rock in coal mining are highly different from the non-karst areas especially at the development height of water-conducting fracture zone (Aladejare et al. 2022; Li et al. 2022; Parise et al. 2004; Waele et al. 2011). Besides, the studies about deformation and failure mechanism of overlying rock under such hydrogeological structure conditions are less not deep yet.

When the fracture zones of roof strata formed after coal mining reach the karst aquifer, the groundwater will enter the mine along them and form mine water inflow(Wu et al. 2024). Over years, under the unremitting efforts with hydrogeological workers, mine water inflow prediction technologies have been greatly developed. Among them, the deterministic calculation method and the non-deterministic calculation method are widely used. The non-deterministic calculation methods mainly include correlation analysis method (Bahrami et al. 2016; Leurgans et al. 1993; Mahdi 2018), gray theory method (Ma and Bai 2015; Rajesh et al. 2014), hydrogeological analogy method (Booshehrian et al. 2020), and neural network method (Hakke et al. 2023; Krivoshchekov et al. 2022), by which a prediction model of mine water inflow is built by using relevant statistical analysis methods based on the measured mine water inflow. These methods all require a large number of hydrogeological parameters, and they are very complicated but with low applicability. The deterministic calculation methods mainly include water balance method (Liu et al. 2016; Zarei et al. 2011), analytical method (Li et al. 2021; Mahmoodzadeh et al. 2021) and numerical method (Butscher 2012; Li et al. 2015). Among them, the water balance method has high requirements on the data acquisition of balance elements

during the balance period (McJannet et al. 2013), and the analytical method has very harsh application conditions, only suitable for mines with simple hydrogeological conditions (Zarei et al. 2011). The numerical method needs a large amount of data to build a calculation model that is consistent with the actual hydrogeological conditions of the mining area. In addition, the existing methodology for predicting mine water inflow typically considers the water-richness of aquifer as the primary factor in calculations, with the influence of the key factor about whether the water-conducting fracture zone reaches the water-rich area of aquifer on the water inflow often being overlooked, which could result in significant discrepancies between the calculated results and the actual test data.

To deeply reveal the deformation and failure characteristics of coal roof strata in karst areas, it is necessary to find a more effective method for predicting mine water inflow. In this paper, similar materials for liquid-solid coupling were first developed, and the coal mining process in karst area was simulated through physical simulation test and numerical simulation. The dynamic failure characteristics of roof strata during the mining process were studied, and the development height of the falling zone and the fracture zone was developed. Based on the above, a three-dimensional numerical model of groundwater flow in a typical coal mine considering the development height of the water-conducting fracture zone was built, and the mine water inflow was predicted. The prediction results were compared with the traditional methods and measured values, and the accuracy of this method was demonstrated. The mine water inflow prediction method considering the development height of the water-conducting fracture zone can more truly reflect the formation mechanism of water inflow, and the prediction process is reasonable, with higher accuracy.

Development of similar materials

Overview of study area

Lvtang Coal Mine (geographical coordinates: E105°20′00″ ~ E105°29′00″, N26°58′00″ ~ N27°09′30″) in Dafang County, Guizhou Province, Southwest China is selected as a typical case. Its geographic location is shown in Fig. 1. This mining area is a typical exposed karst area, and the aquifers are all karst fracture aquifers, which are distributed from top to bottom as follows: the Second Member of Lower Triassic Feixianguan Formation, the Upper Permian Changxing Formation, the Upper Permian Longtan Formation and the Middle Permian Maokou Formation. The water-resisting layers are mainly argillaceous siltstone and siltstone, which are distributed from top to bottom as follows: the third and
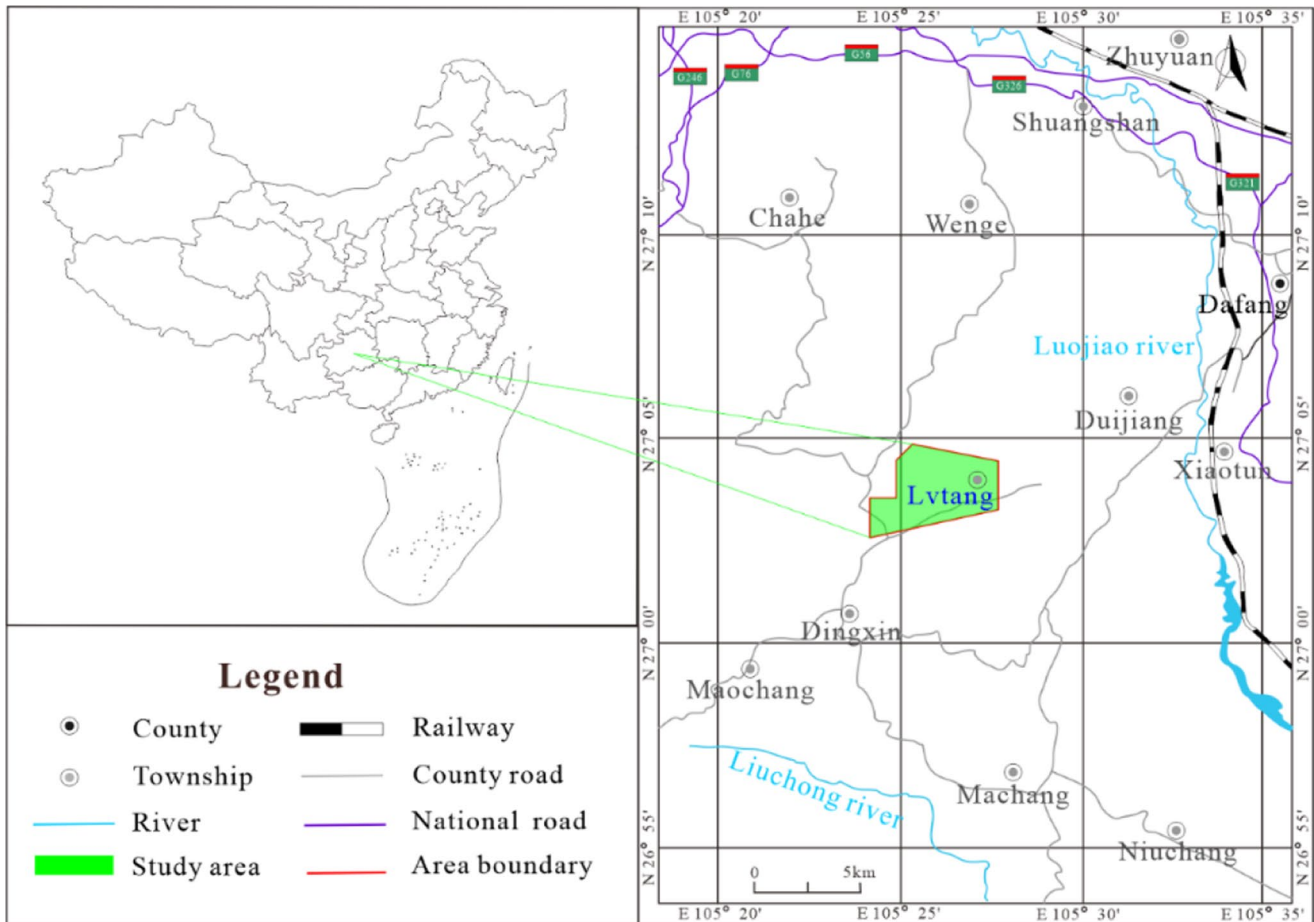
Fig. 1 Geographic location

first members of the Feixianguan Formation, and the argillaceous water-resisting layer in the Longtan Formation, as shown in Fig. 2. The survey data indicates that the primary mining area of Lvtang Coal Mine is 6# coal seam within the Longtan Formation, with an average thickness of 3 m. The aquifers that have a direct water inrush threat to it are Longtan Formation bedrock fissure aquifer and Changxing Formation karst aquifer. Among them, the Longtan Formation stratum is typically composed with thin layers of siltstone, mudstone, and other sedimentary rocks, with multiple layers of thin fractured aquifers (thickness of 0.2~1.64 m). The local fractures of this stratum are more developed, but its water richness is weak. The lithology of the Changxing Formation stratum is mainly medium-thick fine-grained limestone with a thickness of 25~43 m and an average of 28.90 m. Its unit water inflow is 0.023~0.067 L/s·m. The karst development degree of this stratum is notably high, exhibiting considerable variability in water-richness. The local water-richness is relatively strong and primarily based on static reserves. This aquifer also exhibits considerable pressure-bearing characteristic, thereby posing a significant water filling threat to in mining operations. Furthermore, the

aforementioned aquifers are recharged by atmospheric precipitation, and they will also communicate with the overlying aquifer and even surface water as a result of structures and fissures, thus further increasing their water abundance. During process of coal seam mining, the roof strata will collapse and crack, thereby forming a water-conducting fracture zone. If it is connected to the water-rich area of the Changxing Formation aquifer, the risk of a water inrush will be significantly heightened.

Development of similar materials

Based on the similarity criterion, as seen in Eq. (1) ~ (4), the similar materials for each stratum in the study area are developed through orthogonal test. After calculation, the similarity constants of geometry, bulk density, time and strength are 100, 1.5, 10 and 150, respectively. A similarity constant is a ratio of the actual parameter to the simulation parameter.
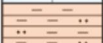
$$C_L = \frac{L_p}{L_m} \tag{1}$$

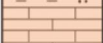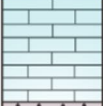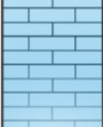| Chronostratigraphic			Stratum code	Lithology columnar	Thickness(m) Min~Max / Average	Lithology characteristics
System	Series	Formation				
Quaternary			Q		$\dfrac{0.80\sim26.87}{15.07}$	Slope sediments Alluvial sediments
Triassic	Lower triassic series	Yongning zhen	T_1yn^1		Incomplete outcrop	Limestone
		Feixianguan	T_1f^3		$\dfrac{32.95\sim66.05}{46.28}$	Mudstone
			T_1f^2		$\dfrac{6.75\sim55.85}{38.45}$	Limestone
			T_1f^1		$\dfrac{48.85\sim200.55}{144.68}$	Siltstone
Permian	Upper permian series	Changxing	P_3c		$\dfrac{13.15\sim14.95}{14.18}$	Limestone
		Longtan	P_3l		$\dfrac{156.05\sim240.55}{214.31}$	Siltstone Mudstone Coal seam
	Middle permian series	Maokou	P_2m		Incomplete outcrop	Limestone

Fig. 2 Stratum structure of Lvtang Coal Mine

$$C_r = \frac{r_1}{r_2} \quad (2)$$

$$C_t = \sqrt{C_L} \quad (3)$$

$$C_\sigma = C_L \times C_r \quad (4)$$

Where C_L, C_r, C_t and C_σ represent the geometric similarity constant, the bulk density similarity constant, the time similarity constant, and the strength similarity constant, respectively; L_p represents the actual size, m; L_m denotes the model size, m; r_1 signifies the actual bulk density of coal rock, N/m³; r_2 represents the bulk density of coal strata in the model, N/m³.

The fine river sand (particle size < 3 mm) is selected as coarse aggregate to increase the strength of the material. The talc powder (purity > 98%) and barite powder ($BaSO_4$ content > 95%) are used as fine aggregates to increase bulk density. The ordinary Portland cement (P30), α-gypsum ($CaSO_4$ content > 99%) and 52# chlorinated paraffin are used as cementitious material to enhance cementation performance. The silicone oil and borax (sodium tetraborate decahydrate, $Na_2B_4O_7 \cdot 10H_2O$) are used as regulators to regulate the plasticity and permeability of the material. The mica powder is used as a layering material to separate the strata. The ratio of similar materials is designed through orthogonal test. Taking the mass ratio of fine river sand to total aggregate (A), the mass ratio of barite powder to fine aggregate (B), the mass ratio of cement to cement (C) and the mass ratio of cement to total mass (D) as factors, and each factor sets five levels. The $L_{25}(5)^6$ orthogonal array is selected to design the test. The factor levels are shown in Table 1. The dry density, uniaxial compressive strength, tensile strength, shear strength and other parameters are regarded as the indexes.

Table 1 Factor levels in orthogonal experiments

Level	Factor			
	Fine river sand/ Total aggregate (A)	Barite powder/ Fine aggregate (B)	Cement/ Cementitious material (C)	Cementitious material/ Total mass (D)
1	91.0%	44.4%	10.0%	6.3%
2	89.7%	53.7%	12.8%	6.5%
3	87.4%	64.0%	15.3%	6.8%
4	85.6%	70.2%	17.6%	7.1%
5	82.8%	76.5%	19.8%	7.4%

Note The cement/gypsum is approximately 2/5; The water consumption is 1/12 of total mass; The borax is 1% of water consumption; The silicone oil is 1/48 of total mass

The test results are shown in Table 2. Through range analysis and comparison with raw materials, the final formula of similar materials in karst strata can be obtained by selecting materials that meet similarity criteria.

It can be seen from Table 2 that the dry density, uniaxial compressive strength, tensile strength and shear strength of similar materials are widely distributed, which can meet the similarity criterion for original rock. By comparing the properties of original rock and selecting the raw material closest to the similarity criterion, the formulas of similar materials for each rock stratum can be obtained. The factor level combination of each formula is shown in Table 3.

Analysis on failure characteristics of overlying rock in coal mining in karst areas

Scheme design

According to the actual geological conditions of Lvtang Coal Mine, a physical simulation test model of 6# coal seam mining was built, as shown in Fig. 3(a). The ratio of this model to actual size was 1:100. The model simulated 150 m

thick strata, including 6# coal. The strata were divided into six layers, from top to bottom, including Feixianguan Formation argillaceous siltstone, Changxing Formation limestone, Longtan Formation argillaceous siltstone, siltstone, 6# coal, argillaceous siltstone. The physical and mechanical parameters of each stratum are presented in Table 4. Due to the height limitation, a vertical uniform load of 107 kPa was applied at the top of hydraulic system to replace the vertical load of upper unsimulated overburden.

In order to monitor the change in stress and displacement of overlying strata during the process of coal seam mining, five monitoring lines had been arranged at an interval of 9 cm above the coal seam, which were recorded as NO.1~NO.5, respectively. Nine displacement sensors and eight stress sensors were arranged on each test line. Two sensors were spaced 11 cm apart. The layout of monitoring points is shown in Fig. 4. Prior to initial use, the sensors were subjected to a series of tests conducted by a multimeter to ascertain their operational functionality. Subsequently, each monitoring position was wiped and polished with alcohol, and then the sensors were installed in turn. It is recommended that the sensors could be positioned vertically upwards in order to monitor the vertical data. Finally, the

Table 2 Test design and results for similar materials

Number	Factor				Dry density (g/cm³)	Uniaxial compressive strength (MPa)	Tensile strength (MPa)	Shear strength	
	A	B	C	D				Internal friction (°)	Cohesive force (MPa)
A	91.0%	44.4%	12.8%	6.8%	1.80	0.83	0.06	32.84	0.065
B	91.0%	53.7%	15.3%	7.1%	1.72	0.62	0.09	35.84	0.033
C	91.0%	64.0%	17.6%	7.4%	1.73	0.68	0.04	28.31	0.068
D	91.0%	70.2%	19.8%	6.3%	1.56	0.43	0.05	29.48	0.023
E	91.0%	76.5%	10.0%	6.5%	1.64	0.32	0.03	21.94	0.067
F	89.7%	44.4%	15.3%	7.1%	1.71	0.41	0.04	32.85	0.035
G	89.7%	53.7%	17.6%	7.4%	1.81	0.54	0.1	38.31	0.068
H	89.7%	64.0%	19.8%	6.3%	1.71	0.18	0.04	35.59	0.031
I	89.7%	70.2%	10.0%	6.5%	1.80	0.44	0.05	34.61	0.024
J	89.7%	76.5%	12.8%	6.8%	1.67	0.48	0.04	32.22	0.042
K	87.4%	44.4%	17.6%	7.4%	1.76	0.18	0.03	29.61	0.035
L	87.4%	53.7%	19.8%	6.3%	1.74	0.38	0.03	22.78	0.053
M	87.4%	64.0%	10.0%	6.5%	1.68	0.32	0.06	32.77	0.035
N	87.4%	70.2%	12.8%	6.8%	1.72	0.28	0.02	29.48	0.024
O	87.4%	76.5%	15.3%	7.1%	1.65	0.26	0.05	33.43	0.026
P	85.6%	44.4%	19.8%	6.3%	1.75	0.19	0.02	33.27	0.031
Q	85.6%	53.7%	10.0%	6.5%	1.69	0.27	0.02	27.44	0.045
R	85.6%	64.0%	12.8%	6.8%	1.72	0.42	0.04	31.12	0.032
S	85.6%	70.2%	15.3%	7.1%	1.83	0.61	0.03	27.53	0.036
T	85.6%	76.5%	17.6%	7.4%	1.78	0.47	0.02	27.21	0.059
U	82.8%	44.4%	10.0%	6.5%	1.79	0.40	0.03	25.59	0.049
V	82.8%	53.7%	12.8%	6.8%	1.64	0.73	0.02	19.87	0.133
W	82.8%	64.0%	15.3%	7.1%	1.75	0.61	0.05	28.38	0.023
X	82.8%	70.2%	17.6%	7.4%	1.74	0.60	0.02	21.26	0.03
Y	82.8%	76.5%	19.8%	6.3%	1.69	0.32	0.03	38.3	0.044

Table 3 Comparison of similar materials and raw rock properties

Stratum	Lithology	Test number	Comparison of properties between original rock and similar materials				Perme- ability (mD)	Material formula
			Density (g/cm^3)	Compressive strength (MPa)	Tensile strength (MPa)	Cohesive force (MPa)		
Feixianguan Formation	Muddy siltstone	N	2.58/1.72	32.67/0.28	3.72/0.02	3.52/0.024	8.36	$A_3B_4C_2D_3$
Changxing Formation	Limestone	L	2.62/1.74	62.23/0.42	9.11/0.05	6.80/0.053	9.35	$A_3B_2C_5D_1$
Longtan Formation	Muddy siltstone	O	2.51/1.65	32.14/0.26	2.19/0.02	3.12/0.026	8.11	$A_3B_5C_3D_4$
	Siltstone	Q	2.55/1.69	38.53/0.27	3.96/0.03	4.20/0.045	8.51	$A_4B_2C_1D_2$
	Muddy siltstone	H	2.56/1.71	26.17/0.18	4.46/0.04	3.16/0.031	8.27	$A_2B_3C_5D_1$
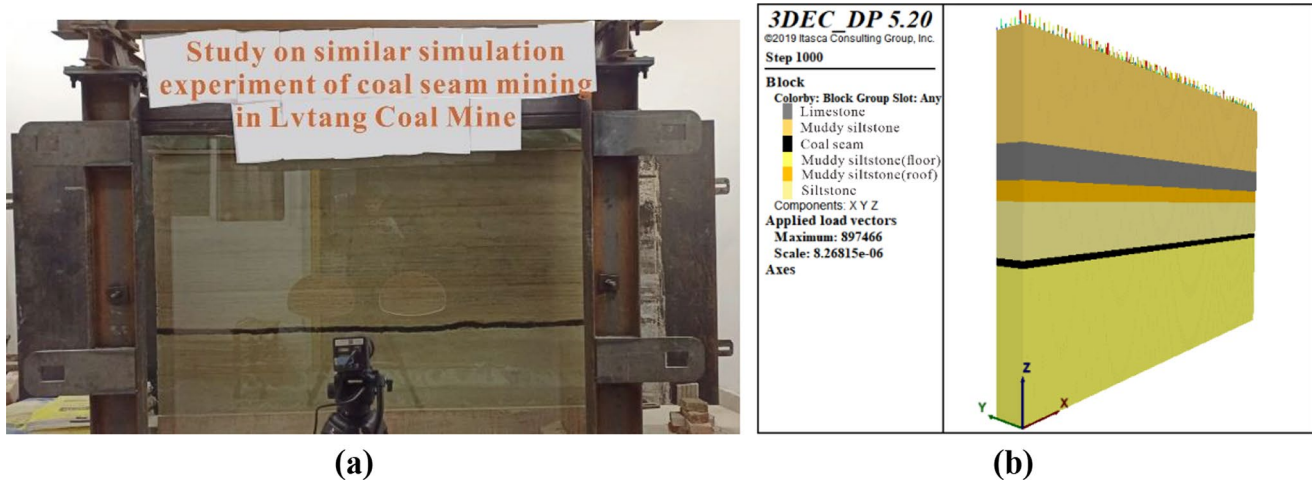
Fig. 3 Physical model and numerical model. (**a**) physical model; (**b**) numerical model

Table 4 Physical and mechanical parameters of each stratum in the model

Stratum	Lithology	Thickness (cm)	Density (g/cm^3)	Compressive strength (MPa)	Tensile strength (MPa)	Elastic modulus (MPa)	Cohesive force (MPa)
Feixianguan Formation	Muddy siltstone	43	1.72	0.28	0.02	135	0.024
Changxing Formation	Limestone	14	1.74	0.42	0.05	364	0.053
Longtan Formation	Muddy siltstone	8	1.65	0.26	0.02	306	0.026
	Siltstone	22	1.69	0.27	0.03	147	0.045
	6# coal seam	3	-	-	-	-	-
	Muddy siltstone	60	1.71	0.18	0.04	121	0.031

Note The 6# coal seam is replaced by a wood strip with a thickness of 3 cm, and the coal seam mining is simulated by pulling out the wood strip during the test

sensors were connected to the test and analysis system, and the initial parameters were cleared and calibrated. The coal pillars with 30 cm were retained on the left and right sides of coal seam, and the coal was mined sequentially from left to right during mining. The mining distance was 2 cm each time, and the next mining started after 0.5 h. The coal was mined for a total of 80 times, with a total mining distance of 160 cm.

As the physical simulation test is unable to visually display the changes of the overlying rock plastic zone, but which can be presented in the form of a numerical simulation. In this study, the 3DEC software was employed to numerically simulate and analyze the dynamic changes of the plastic zone during coal seam mining. Based on the comprehensive histogram of the strata in Fig. 2, a numerical model of 6# coal seam mining in Lvtang Coal Mine was
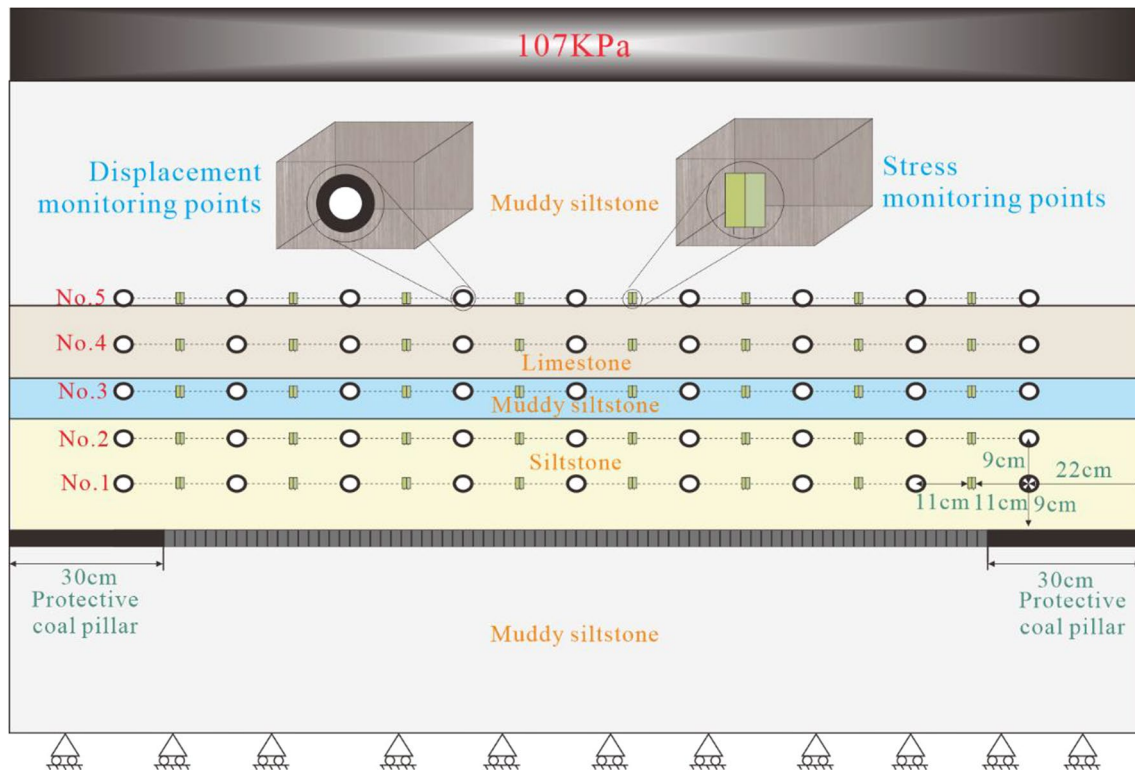
Fig. 4 Layout of monitoring points

constructed, as illustrated in Fig. 3(b). To facilitate a more robust comparison between the numerical and physical simulations, the stratigraphic configuration and thicknesses in the numerical model were aligned with those in the physical model. From top to bottom, the strata were comprised of argillaceous siltstone of the Feixianguan Formation, limestone of the Changxing Formation, argillaceous siltstone, siltstone, 6# coal seam, and argillaceous siltstone of the Longtan Formation. The physical and mechanical parameters of each stratum were presented in Table 3, which listed the original rock parameters. Overall, the length, width, and height of numerical model were 220 m, 15 m, and 150 m, respectively. To ensure the safety of mining operation, protective coal pillars measuring 30 m in length have been left at both ends along the direction of coal seam mining. The model was meshed using tetrahedral elements, with a total of 5,341,846 cells divided. The Mohr-Coulomb criterion was employed for the calculation. The boundary conditions of four sides and bottom of the model were constrained. Among them, the horizontal direction of the sides and the bottom were set to fixed displacement, while the top surface was set to a free boundary. A vertical load of 16.05 MPa was applied to the top of model in order to simulate the effect of upper overburden gravity. Upon excavation of the coal seam, it was set to be excavated 2 m every 420 steps, for a total of 33,600 steps. The layout of monitoring points was consistent with that of the physical simulation test, as

illustrated in Fig. 4. The vertical displacement and stress data of each measuring point during coal seam excavation were monitored and recorded.

Results and discussion

Deformation and failure characteristics of overlaying rock

The coal seam was mined step by step according to the above test scheme. The deformation and failure of the overlying rock at each mining stage is shown in Fig. 5. It can be seen that, on the whole, with the mining of the coal seam, the roof of the initial mining area is almost completely collapsed, and the overlying rock in the later mining area is suspended. When the coal seam is mined to 40 cm, as shown in Fig. 5(a), transverse fractures with lengths of 18 cm and 6 cm appear in the overlying rock at 3 cm and 7 cm above the coal seam. No vertical cracks were seen. Small overlying rock deformation was seen and no collapse occurred. This was because the coal seam roof formed a cantilever beam structure at this time and had not yet reached the limit breaking distance, so the roof had not reached the caving condition. The early transverse cracks further developed into bed-separated fractures with a length of 65 cm and a maximum width of 0.4 cm. This was because when the coal mining distance increased, beyond the protection range of the coal pillar, the overlaying rock collapsed under gravity of the overlying
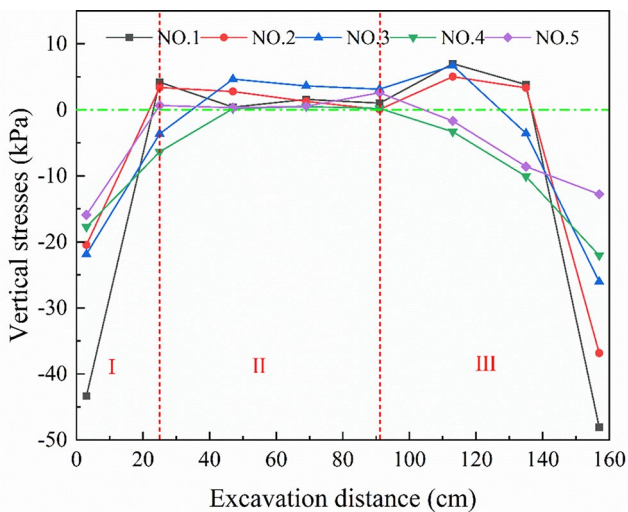
(a)

(b)

(c)

(d)
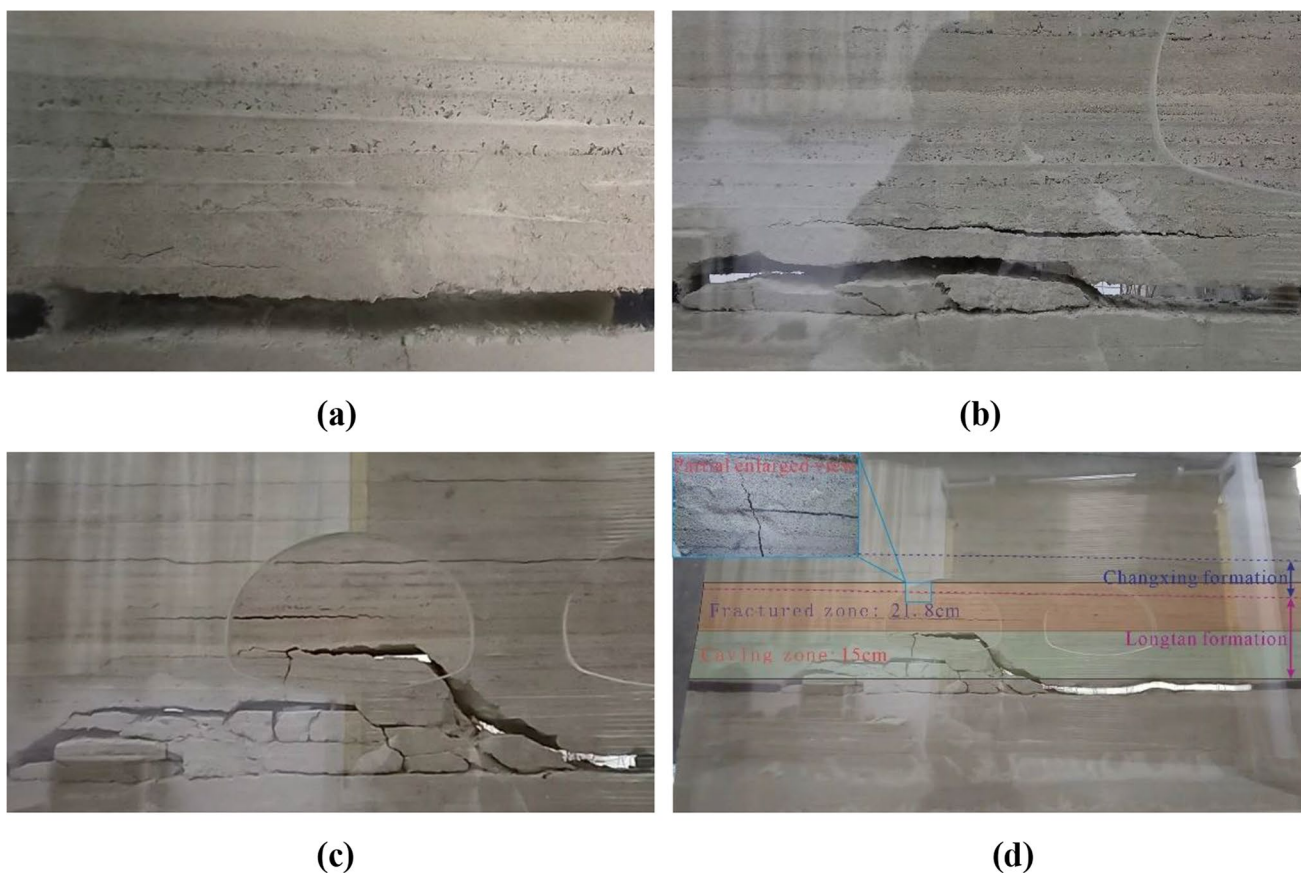
Fig. 5 Deformation and failure of overlying rock in coal mining. (**a**) mining distance 40 cm; (**b**) mining distance 80 cm; (**c**) mining distance 120 cm; (**d**) mining distance 160 cm

strata. When the coal seam was mined to 120 cm (as shown in Fig. 5(c)), the overlying rock further fractured and collapsed, and the height of falling zone increased to 15 cm. A new transverse fracture developed above the falling zone, with a length of 78 cm and a maximum width of 0.4 cm. At this time, no vertical fissures have developed yet. When the coal seam was fully mined (160 cm) (as shown in Fig. 5(d)), no new overlying rock collapsed, and the roof shape tended to be stable. The interlayer fracture continued to develop horizontally to 103 cm, but closed vertically. At this time, a vertical fracture appeared directly above the transverse fracture, with a length of 16.8 cm and a maximum width of 0.2 cm, which was because when the roof collapsed in a large area, the overlying rock was less supported, resulting them bent and damaged, thus the vertical fractures were generated under tension. In the end, the height of falling zone and fracture zone was 15 cm and 21.8 cm respectively, totaling to 36.8 cm. It can be seen that these 'two zones' have developed to the middle and lower part of Changxing Formation aquifer.
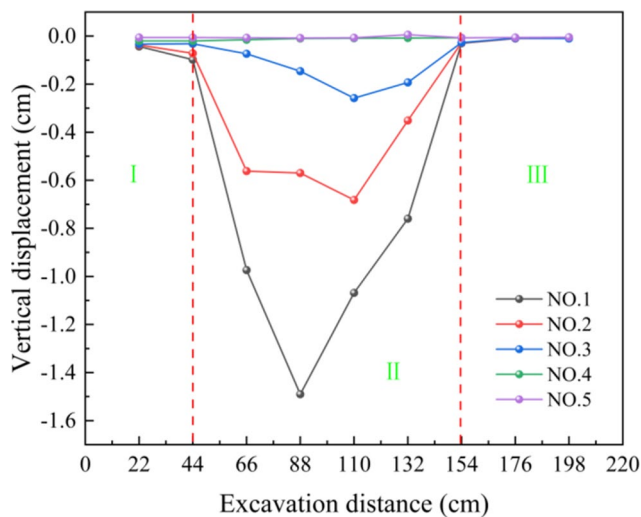
Stress change characteristics of overlaying rock

After coal mining (160 cm), the stress distribution of overlaying rock along the mining direction is shown in Fig. 6. In the figure, the positive value indicates that the stress increases while the negative value indicates that the stress decreases. It can be seen from Fig. 6 that when the coal seam on the working face is fully mined, the change in the stress of the overlying strata in the goaf along the mining direction can be divided into three areas, including increasing stress area, stable stress area and decreasing stress area, corresponding to areas I, II, and III in Fig. 6. The stress values in areas I and III are almost all negative, and the stress values in area II are all positive and close to 0. In addition, the stress difference of each monitoring line at different heights from the coal roof is also different. The stress differences of monitoring lines NO.1 to NO.5 are 55.06 kPa, 41.86 kPa, 32.72 kPa, 22.54 kPa and 18.51 kPa, respectively. It can be seen that the farther away from the coal seam in the vertical direction, the smaller the stress change of the overlying rock.

It can be seen from Fig. 5 that with the mining of the coal seam, the scope of goaf gradually increases, resulting in an increase in the hanging distance of the roof. When

Fig. 6 Vertical stress at each measuring point at coal mining distance of 160 cm

Fig. 7 Vertical displacement at each measuring point at coal mining distance of 160 cm

the collapsed rock in the left goaf and the right coal seam. Consequently, as a result of coal seam mining, the roof stress in this area is unloaded, exhibiting a downward trajectory. In general, the closer the distance from the coal seam, the greater the stress change of the overlying strata. This is due to the fact that the goaf is formed subsequent to coal seam mining. As the overlying strata become closer to the goaf, the gravity of the overlying strata increases, while the supporting force of the lower part decreases. Consequently, the stress differential is the most pronounced and susceptible to collapse. The farther away from the goaf is the rock formation, the less pressure it receives and the greater the supporting force, the relatively more stable and less likely to be damaged.

Change characteristics of overlying rock displacement

After coal mining (160 cm), the change of overlaying rock displacement along the mining direction is shown in Fig. 7. The overlying rock can also be divided into three zones by overall displacement distribution, namely stable displacement zone, displacement changement zone and stable displacement zone, which correspond to areas I, II and III in Fig. 7, respectively. Among them, the overlying rocks in areas I and III hardly move. In area II, the displacement of overlying rock on NO.1, NO.2 and NO.3 monitoring lines shows a trend of first increasing and then decreasing, while the displacement of overlaying rock on NO.4 and NO.5 monitoring lines hardly occurs. On the whole, the closer to the coal roof, the greater the displacement change of the overlying rock. The displacement differences of NO.1~NO.5 monitoring lines are 1.48 cm, 0.67 cm, 0.25 cm, 0.01 cm and 0 cm, respectively. It can be seen that there is almost no displacement of overlying rock to No.4 monitoring line (36 cm from the coal roof), which also reflects that the development height of two zones is about 36 cm, which is consistent with the results shown in Fig. 5(d). The reason is that coal pillars exist near areas I and III, and acts as a support for the overlying rock. Therefore, the overlying rock is relatively stable and no large displacement has occurred. Area II is far away from the coal pillar, and the overlying rock loses its support. Under the gravity of the overlying strata, the overlying rock will be damaged and undergo large displacement. The closer to the middle area of working face, the farther away from the coal pillar, and the greater the deformation of overlying rock. In the overall vertical direction, the closer the overlying rock is to the coal roof, the greater the gravity of the overlying rock is, also the greater the displacement change. When the overlying rock is far enough away from the roof (above the NO.4 monitoring line), the lower strata are sufficient to support the overlying strata, so that

it exceeds the limit caving distance, the roof will collapse. Due to the area I is the first mining area, after the coal seam is mined, the overlying rock unloads and the stress will decrease rapidly. Coupled with the existence of the left coal pillar, the overlying rock closer to the coal pillar is more difficult to collapse, and the unloading stress is not easy to recover. Therefore, the area I shows a trend of decreasing with the degree of stress unloading away from the coal pillar. Due to far away from the coal pillar, the gravity of the overlying strata in area II will be redistributed and act on the caving strata. Under partial tensile stress, the overall stress in this zone is close to the original stress but slightly greater than the original stress. Area III is the final mining area. The overlying strata have not undergone complete collapse, with some remaining in a suspended state, due to the support of

the overlying rock is stable and the displacement will no longer change.

Change characteristics of overlaying rock plastic zone

The plastic zone can reflect the overlying rock failure. To show the change of overlying rock plastic zone more intuitively, the numerical simulation was done by using 3DEC software. The changes in the overlaying rock plastic zone in coal mining are shown in Fig. 8. It can be seen that when the coal seam was mined to 40 m (as shown in Fig. 8(a)), the plastic zone just began to develop, and it was very small and distributed along the mining direction in a spotty pattern. It showed that the overlying rock was still relatively stable at this time, and no extensive damage occurred. This was consistent with the overlying rock morphology in Fig. 5(a). When the coal seam was mined to 80 m (as shown in Fig. 8(b)), the overlaying rock plastic zone on the working face expanded and gradually increased. On the side of the open-off cut, some coal pillars and the overlying rock plastic zone began to develop, which was because the damage to overlying rock by coal mining gradually appeared far away from the coal pillar. Due to support loss of coal pillar and mining, the roof overlying rock on one side of

the working face was damaged, resulting in the continuous expansion of the plastic zone. On the side of the coal pillar adjacent to the goaf, due to the continuous increase of gravity and horizontal stress, the bearing limit of the coal pillar and overlying rock was gradually exceeded, and the plastic zone was developed. When the coal seam was mined to 120 m (as shown in Fig. 8(c)), the plastic zone had been widely developed above the entire goaf. The plastic zone located in the middle left of the goaf had been connected with each other and developed to the coal floor. This phenomenon showed that the roof had collapsed and filled to the goaf. The plastic zone near the coal pillar and the working face was also further developed in the horizontal and vertical directions. When the coal seam was mined to 160 m (as shown in Fig. 8(d)), the plastic zone in the middle of the goaf had been fully developed and connected with each other. It can be seen that the overlying rock had collapsed in a large area at this time, forming a falling zone, to fill the goaf. A vertically connected plastic zone was distributed near the coal pillar above the falling zone, while a horizontally nearly connected plastic zone was distributed on the side of working face. It showed that vertical and horizontal fractures were widely developed in these zones, forming a fracture zone. This was consistent with the results in
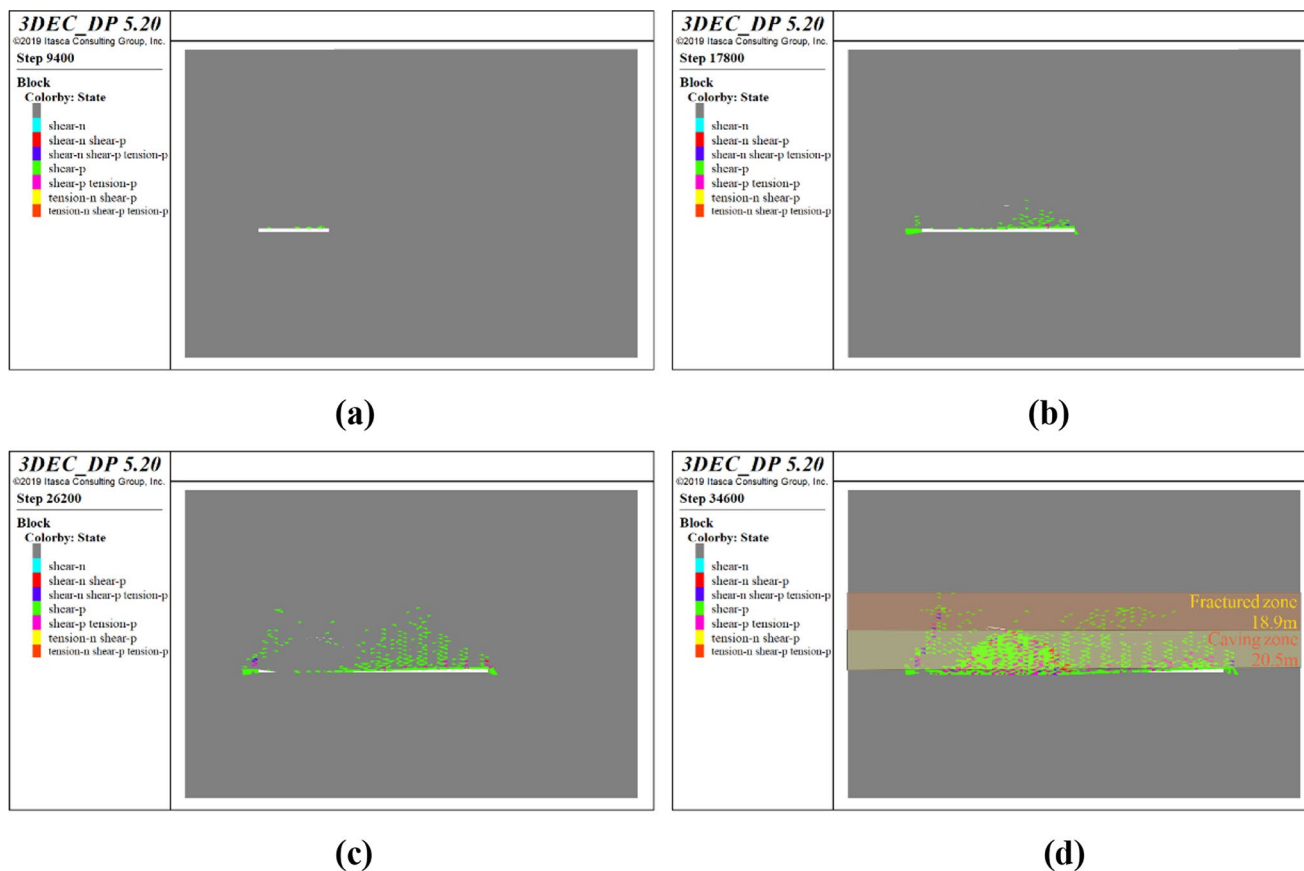

Fig. 8 Changes in overlaying rock plastic zone during coal mining. (**a**) mining 40 m; (**b**) mining 80 m; (**c**) mining 120 m; (**d**) mining 160 m

Fig. 5(d). Finally, the total development height of overlying rock plastic zone was 39.4 m, of which the height of the falling zone was 20.5 m, and the height of the fracture zone was 18.9 m.

Development height of "two zones" on coal roof in karst area

The total height of falling zone and fracture zone ('two zones') from physical simulation tests is 36.8 m, and that calculated by numerical simulation is 39.4 m. To verify the accuracy of these results, it is calculated by the empirical formula in the Chinese national code - *Code for Coal Pillar Retention and Coal Mining in Buildings*, *Water Bodies*, *Railways and Main Shafts* (General Administration of State Safety Supervision 2017). The coal roof of Lvtang Coal Mine is medium-hard rock with a uniaxial compressive strength of 38.53 MPa, so the empirical Eqs. (5) and (6) are used. By substituting the coal thickness of 3 m into Eqs. (5) and (6), the total height of the 'two zones' is ranged from 36.97 to 52.57 m, with an average of 44.77 m.

$$H_k = \frac{100 \sum M}{4.7 \sum M + 19} \pm 2.2 \tag{5}$$

$$H_{li} = \frac{100 \sum M}{1.6 \sum M + 3.6} \pm 5.6 \tag{6}$$

Where H_k is the height of falling zone, m; H_{li} is the height of water-conducting fracture zone, m; $\sum M$ is the cumulative mining thickness, m.

The development height of the 'two zones' from physical simulation test and numerical simulation analysis is close to the minimum value calculated by empirical formula, and smaller than its average value. The main reason is that the applicability of the empirical formula is limited, and the limestone widely distributed on the coal roof in Southwest China has higher mechanical strength and better stability. The model built during physical simulation test and numerical simulation analysis is more in line with the actual geological conditions of Lvtang Coal Mine, and more factors are taken into consideration. This paper chooses a relatively conservative value 39.4 m as the final result about the development height of 'two zones'.

Prediction of mine water inflow considering the development height of water-conducting fracture zone

Numerical prediction model and result analysis

3D geological model building

Mine water inflow prediction is an important basis for mine planning, design and safe. A three-dimensional unsteady flow numerical model of groundwater in mining areas is built by using GMS software to dynamically predict the mine water inflow during mine mining. The simulation area is delimited by non-natural boundary processing method, with an area of about 24 km^2. According to the aquifer hydrogeological conditions and characteristics, the model is generalized into a three-layer structure in the vertical direction. The first layer is Feixianguan Formation and Quaternary strata, which can be generalized as impermeable phreatic aquifer. The second layer is Changxing Formation strata, which is generalized as a permeable aquifer. The third layer is Longtan Formation, which is generalized as the water-repellent bottom boundary. The geological drilling data of previous exploration are imported into the model in layers, and a 3D geological entity is generated by the inverse distance weighting interpolation method, as shown in Fig. 9. According to the hydrogeological data, the flow boundary and water-repellent boundary are set. The groundwater recharge in the study area is dominated by atmospheric precipitation and lateral inflow. The discharge methods are mainly mining water pumping, seasonal gully, spring, and lateral outflow. The source sink term parameters of the model are set accordingly.

Setting of water-conducting fracture zone

The coal seam of Lvtang Coal Mine is located in the Longtan Formation aquifer, which effectively prevents water from the top aquifer of Changxing Formation from entering the mine. The water-conducting fracture zone formed after coal mining also develops from this layer. Once the water-conducting fracture zone develops to the aquifer of Changxing Formation, the barrier effect on the groundwater will be destroyed and a water inflow channel will be formed. Therefore, the influence of water-conducting fracture zone must be considered in the prediction of mine water inflow. According to the elevation of aquifer floor, the elevation of the coal roof, and the height of water-conducting fracture zone, the Longtan Formation aquifer is divided into three zones, as shown in Fig. 10. Among them, area I is a zone where the water-conducting fracture zone has not developed to the aquifer, and the water-repellent layer in this
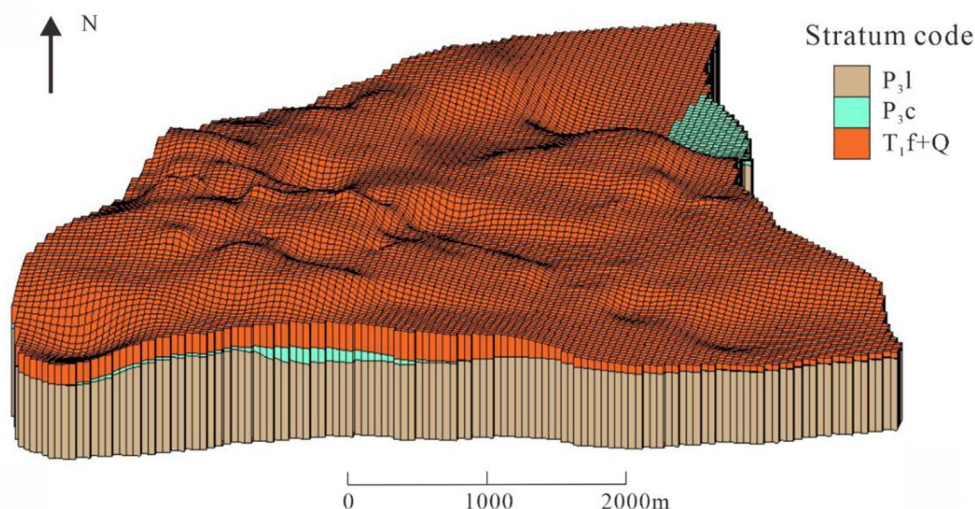
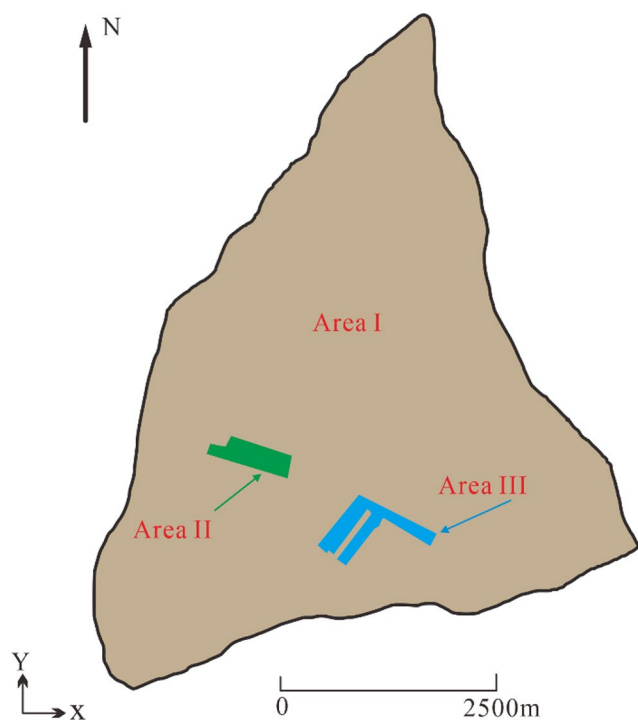**Fig. 9** 3D hydrogeological model building

Fig. 10 Partition of water-conducting fracture zone

Table 5 Hydrogeological parameters of each division of the Longtan formation strata

Parameter	Area I	Area II	Area III
Lateral permeability coefficient (m/d)	0.065	10.84	5.332
Longitudinal permeability coefficient (m/d)	0.0127	20.05	7.405
Water storage rate (1/m)	0.000046	0.008915	0.0037

parameters of area III to increase its water conductivity. The groundwater flow field changes in the study area from May 2018 to October 2020 are simulated and checked with the actual monitoring results. The final hydrogeological parameters of the three zones are shown in Table 5.

Numerical model prediction of mine water inflow

According to the mining plan of Lvtang Coal Mine from 2021 to 2025, pumping wells are equivalently arranged according to the position, depth, shape and area of the roadway and mining face to ensure that water is pumped to the entire mining area. Assuming that the equivalent pumping well continues to pump water, the water level of Changxing Formation aquifer is dredged down to the elevation of coal floor (safety water level). When the pumping volume reaches a steady state, the total pumping volume of the pumping well is the mine water inflow. The mine water inflow during coal seam mining from January 2021 to December 2025 is predicted. Among them, the water level distribution of the Changxing Formation aquifer in 2025 is shown in Fig. 11, and the prediction results of annual mine water inflow are shown in Fig. 12.

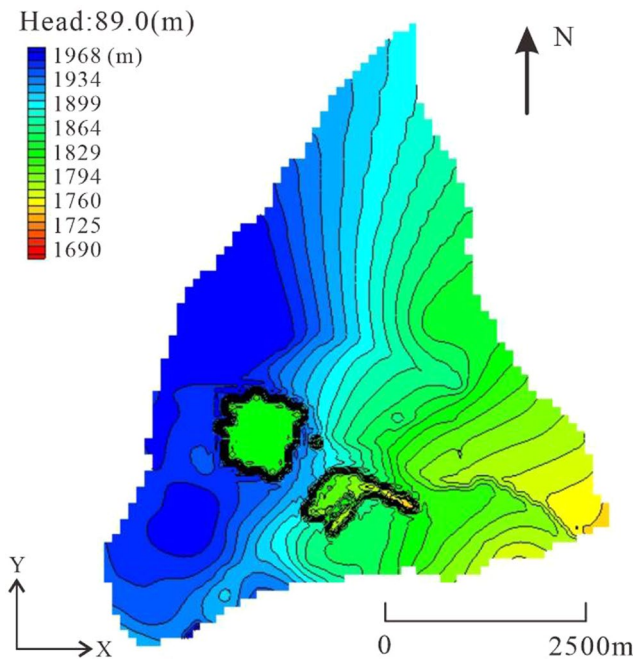It can be seen from Fig. 11 that in areas II and III of Fig. 10, a groundwater depression cone centered on the

zone has good water-repelling performance but poor water-conducting capacity. Areas II and III are the two zones where the water-conducting fracture zone develops to the aquifer respectively. In these zones, rock mass fractures are developed and the water-repelling performance is poor. The average thickness of aquifer in area II is 27.95 m, which is lower than 29.55 m in area III. The fractures in the aquifer are more broken and the water conductivity is stronger. Therefore, the hydrogeological parameters of area II need to be multiplied by a certain coefficient on the basis of the

Fig. 11 Water level distribution of Changxing Formation aquifer
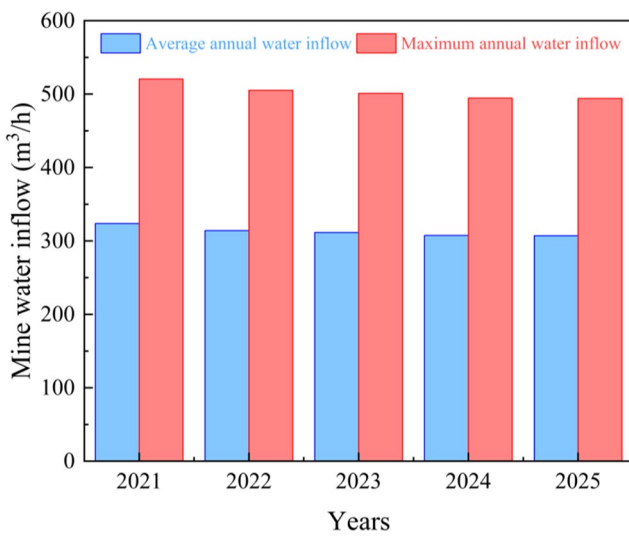

Fig. 12 Changes in mine water inflow from 2021 to 2025

mining face is formed. This is because the water-conducting fracture zone generated during coal mining develops to the Changxing aquifer, so that a large amount of groundwater in the aquifer flows into the mine, and the water level in the corresponding zone of aquifer continues to decline. It can be seen from Fig. 12 that from 2021 to 2025, the mine water inflow will show a slow downward trend, and the rate of decline will gradually slow down, and finally tend to be stable. After stable, the average annual water inflow of the mine is 307 m³/h, and the annual maximum water inflow is 494 m³/h.

Other methods

Big well method

The basic principle of the big well method is to generalize the roadway and the working face into a big well with similar shape, and the area of the big well is the total area of roadway and goaf. Hence, the mine water inflow can be converted into the big well water inflow (Shi 2019; Zaidel et al. 2010), as shown in Eq. (7) ~ (9).

$$r = \sqrt{F/\pi} \tag{7}$$

$$R = r + 10s\sqrt{K} \tag{8}$$

$$Q = \frac{\pi K[(2H - M)M - h_0^2]}{lnR - lnr} \tag{9}$$

Where Q is the mine water inflow, m³/d; F is the calculated area, m²; K is the permeability coefficient, m/d; s is the water level drawdown, m; H is the static head elevation, m; M is the thickness of the aquifer, m; h_0 is the distance from the initial water level to coal floor, m; R is the influence radius, m; r is the reference radius, m.

BP neural network

The BP neural network prediction model consists of three layers, which are input layer, hidden layer and output layer. Among them, the hidden layer is the most important building block in the prediction model (Jiao 2010). To make the prediction model more accurate, this study sets the number of hidden layers to 2, and the number of units on each hidden layer to 100. The model keeps going forward, and iterates the amount of information in the historical time back in a linear transmission manner, and then determines the next input and output. The input gate output signal i_t, the hidden layer state h_t, and the output gate output signal O_t are calculated by Eqs. (10) ~ (12) (Ren et al. 2014).

$$i_t = S(Q_{ix}x_t + Q_{ih}h_{t-1} + q) \tag{10}$$

$$h_t = O_t \cdot tanh(d_t) \tag{11}$$

$$O_t = S(Q_{ox}x_t + Q_{oh}h_{t-1} + q_o) \tag{12}$$

Where x_t represents the current input; d_t represents the long-term memory state; Q_{ix}, Q_{ih}, Q_{ox} and Q_{oh} are corresponding weight matrices; q_i and q_o are bias matrices; S is the *sigmoid* function.

Table 6 Prediction results of mine water inflow

Date	Measured value (m³/h)	Big well method (m³/h)	BP neural network method (m³/h)
2021.01	167.7	373.9	238.7
2021.02	201.7	454.5	288.8
2021.03	317.6	452.7	297.7
2021.04	397.4	482.0	401.4
2021.05	432.8	478.0	316.6
2021.06	564.7	497.0	358.4
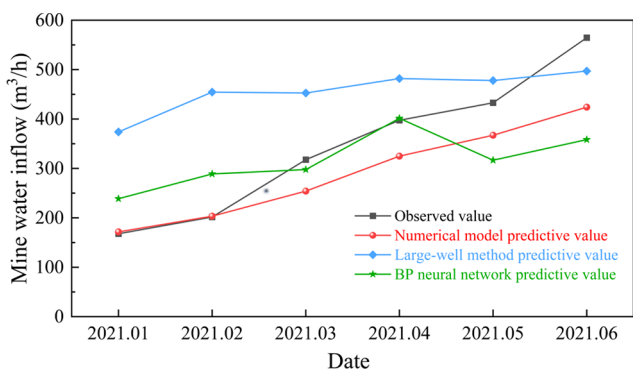
Fig. 13 Comparison of prediction results of mine water inflow by different methods

Prediction results

The monthly water inflow of the mine from January to June 2021 is calculated using big well method and BP neural network method. The results are shown in Table 6. It can be seen that the average water inflow predicted by big well method is 456.35 m³/h, and that predicted by BP neural network method is 316.93 m³/h.

Comparative analysis of prediction methods

The results of the mine water inflow predicted by the numerical model, the big well method and BP neural network method from January to June 2021 are compared with the measured values, and the results are shown in Fig. 13. It can be seen that the prediction results of numerical model are closest to the change trend of the measured values, showing a trend of increasing month by month. The prediction results of big well method only show a large initial increase and then a slow increase, while the prediction results of BP neural network method show a trend of first increasing, then decreasing and then increasing, both of which are quite different from the measured values. By comparing the prediction results of 6 months with the measured values the maximum error of the numerical model is 140.7 m³/h, with an error rate of 24.92%, but that of big well method and BP neural network are 252.8 m³/h and 206.3 m³/h, with an error

rate of 125.33% and 36.53%, respectively. It can be seen that the numerical model has the maximum prediction accuracy, while the big well method has the minimum prediction accuracy. It can also be found that the prediction results of big well method are generally greater than the measured values, only slightly smaller in June. This is because the large well method regards the entire mining area as a water-conducting channel, and does not consider the key factor of whether the water-conducting fracture zone is connected to aquifer, so the prediction value is too large. However, the rainy season appears in June, when water is largely recharged by atmospheric precipitation. The big well method cannot consider the factor of precipitation recharge, so the prediction value in June is slightly smaller than the measured value. The prediction results of BP neural network method vary greatly, which will greatly reduce the stability of prediction effect. This is because there are many factors affecting mine water inflow, and BP neural network cannot consider the characteristics of water inflow controlled by multiple factors during prediction. The prediction results of numerical simulation method are closest to the measured values, because the numerical model takes into account the key criterion of whether the water-conducting fracture zone develops to the aquifer, which is consistent with the actual mining conditions. It should be noted that due to the simplification of the model, this paper does not take into account the fact that a small amount of groundwater in the aquifer enters the mine, leading to that the prediction results are slightly smaller than the measured values.

Conclusions

(1) A large number of similar material preparation schemes are designed through orthogonal test. With dry density, uniaxial compressive strength, tensile strength and shear strength as similar parameters, a new similar material formula suitable for physical simulation test of coal mining in exposed karst area is developed through testing and analysis, and it is composed of fine river sand, talc powder, cement, gypsum, barite powder, chlorinated paraffin, borax and silicone oil. Based on the above, according to the geological background of typical coal mines, a physical simulation model of roof rock formation failure in coal mining is built to dynamically monitor the stress, displacement and deformation failure characteristics.

(2) Through physical simulation test and numerical simulation analysis, the failure characteristics of the coal roof strata in coal mining are studied. It is found that at the beginning of mining, due to the existence of coal pillars, the overlaying rock does not collapse, and the plastic zone only develops and accumulates near the coal roof. When the

mining distance is greater than the support range of coal pillar, the plastic zone of overlying rock develops in a large area and is connected with each other, and then collapses and fills the goaf. After mining, the roof of the initial mining section all collapses, the plastic zones are connected to each other, and transverse and vertical fractures are widely developed. The overlying rock can be divided into three areas along the mining direction by stress and displacement, which are mainly determined by the horizontal distance between the position, coal pillar, and the vertical distance of the goaf. Due to the widespread distribution of limestone with high mechanical strength on the coal roof in the exposed karst area, the development height of 'two zones' in coal mining is slightly lower than that in other areas.

(3) The existing mine water inflow prediction methods take mining area and historical water inflow data as the main basis for the prediction of mine water inflow, and the calculation process does not accurately reflect the formation process of mine water inflow. Based on the development height of water-conducting fracture zone and groundwater flow model, a three-dimensional numerical model for predicting mine water inflow is built, and the water inflow of typical coal mines is predicted. Through comparative analysis with the big well method, BP neural network method and the measured values, it can be found that the numerical simulation method considering the height of water-conducting fracture zone has the minimum error in prediction results and the maximum accuracy. Its results are the closest to the measured value, which can more truly reflect the dynamic formation process of mine water inflow. In addition, the prediction results of numerical simulation method are slightly lower than the measured values. In the future, the recharge water in the coal measure aquitard can be considered to be added to the model to further improve the prediction accuracy.

Data availability Data will be made available on request.

Declarations

Conflicts of interest The authors declare that they have no conflicts of interest.

References

Aladejare AE, Ozoji T, Lawal AI, Zhang ZX (2022) Soft computing-based models for predicting the characteristic impedance of igneous rock from their physico-mechanical properties. Rock Mech Rock Eng 55(7):4291–4304. https://doi.org/10.1007/s00603-022-02836-5

Bahrami S, Ardejani FD, Baafi E (2016) Application of artificial neural network coupled with genetic algorithm and simulated annealing to solve groundwater inflow problem to an advancing open pit mine. J Hydrol 536:471–484. https://doi.org/10.1016/j.jhydrol.2016.03.002

Booshehrian A, Wan R, Su XQ (2020) Hydraulic variations in permafrost due to open-pit mining and climate change: a case study in the Canadian Arctic. Acta Geotech 15(4):883–905. https://doi.org/10.1007/s11440-020-01079-4

Butscher C (2012) Steady-state groundwater inflow into a circular tunnel. Tunn Undergr Space Technol 32:158–167. https://doi.org/10.1016/j.tust.2012.06.007

Erguler ZA, Ulusay R (2009) Water-induced variations in mechanical properties of clay-bearing rocks. Int J Rock Mech Min Sci 46(2):355–370. https://doi.org/10.1016/j.ijrmms.2008.07.002

Feng SJ, Zhao XF, Sun SG (2014) The numerical simulation of overburden strata failure law by full-mechanized caving mining in extra thick coal seams. Adv Mater Res 962–965:1179–1182. https://doi.org/10.4028/www.scientific.net/AMR.962-965.1179

General Administration of State Safety Supervision, State Administration of Coal Mine Safety Supervision and State Energy Administration (2017) Specifications for coal pillar retention and coal mining in buildings, water bodies, railways and main roadways. Coal Industry Publishing House (China)

Guo H, Adhikary DP, Craig MS (2009) Simulation of mine water inflow and gas emission during longwall mining. Rock Mech Rock Eng 42(1):25–51. https://doi.org/10.1007/s00603-008-0168-9

Hakke VS, Gaikwad RW, Warade AR, Sonawane SH, Boczkaj G, Sonawane SS, Sapkal VS (2023) Artificial neural network prophecy of ion exchange process for Cu (II) eradication from acid mine drainage. Int J Environ Sci Technol 20:13479–13490. https://doi.org/10.1007/s13762-023-04818-8

Huang Z, Jiang ZQ, Tang X, Wu XS, Guo DC, Yue ZC (2016) Insitu measurement of hydraulic properties of the fractured zone of coal mines. Rock Mech Rock Eng 49(2):603–609. https://doi.org/10.1007/s00603-015-0741-y

Islam MR, Shinjo R, Faruque MO, Shimada H, Howladar MF (2016) Finite element method (FEM) groundwater inflow modeling associated with an unconfined aquifer into the open-pit coalmine of the Phulbari area, NW Bangladesh. Arablan J Geosci 9(5):394. https://doi.org/10.1007/s12517-016-2402-1

Jiao L (2010) QSPR studies on soot-water partition coefficients of persistent organic pollutants by using artificial neural network. Chemosphere 80(6):671–675. https://doi.org/10.1016/j.chemosphere.2010.04.013

Krivoshchekov S, Kochnev A, Ozhgibesov E (2022) The application of neural networks to forecast radial jet drilling effectiveness. Energies 15(5):1917. https://doi.org/10.3390/en15051917

Lawson HE, Tesarik D, Larson MK, Abraham H (2017) Effects of overburden characteristics on dynamic failure in underground coal mining. Int J Min Sci Technol 27(1):121–129. https://doi.org/10.1016/j.ijmst.2016.10.001

Leurgans SE, Moyeed RA, Silvermant BW (1993) Canonical correlation analysis when the data are curves. J Roy Stat Soc 55(3):725–740. https://doi.org/10.1111/j.2517-6161.1993.tb01936.x

Li CC, Xu SG, Ba JJ (2015) The prediction of the water inflow by numerical simulation methods of Huijiabao Mine, Guizhou

Province. Appl Mech Mater 744–746:1161–1164. https://doi.org/10.4028/www.scientific.net/AMM.744-746.1161

Li JB, Wang YH, Tan ZS, Du W, Liu ZY (2021) Study on water inflow variation law of 1 shaft auxiliary shaft in highligongshan based on dual medium model. Symmetry 13(6):930. https://doi.org/10.3390/sym13060930

Li B, Zhang WP, Long J, Fan J, Chen MY, Li T, Liu P (2022) Multi-source information fusion technology for risk assessment of water inrush from coal floor karst aquifer. Geomatics Nat Hazards Risk 13(1):2086–2106. https://doi.org/10.1080/19475705.2022.2108728

Li B, Wu H, Liu P, Fan J, Li T (2023) Construction and application of mine water inflow prediction model based on multi-factor weighted regression: Wulunshan Coal Mine case. Earth Science Informatics 16: 1879–1890 https://link.springer.com/article/10.1007/s12145-023-00985-x

Liu WB, Wang L, Zhou J, Li YZ, Sun FB, Fu GB, Li XP, Sang YF (2016) A worldwide evaluation of basin-scale evapotranspiration estimates against the water balance method. J Hydrol 538:82–95. https://doi.org/10.1016/j.jhydrol.2016

Ma D, Bai HB (2015) Groundwater inflow prediction model of karst collapse pillar: a case study for mining-induced groundwater inrush risk. Nat Hazards 76(2):1319–1334. https://doi.org/10.1007/s11069-014-1551-3

Ma M, Liu ZB, Ma XM, Zhao RJ, Mao DQ (2022) Exploration of Ordovician limestone aquifer heterogeneity with tomographic water releasing tests. J Hydrol 608:127655. https://doi.org/10.1016/j.jhydrol.2022.127655

Mahdi RM (2018) Groundwater seepage rate (GSR) a new method for prediction of groundwater inflow into jointed rock tunnels. Tunn Undergr Space Technol 71:505–517. https://doi.org/10.1016/j.tust.2017.10.006

Mahmoodzadeh A, Mohammadi M, Noori KMG, Khishe M, Ibrahim HH, Ali HFH, Abdulhamid SN (2021) Presenting the best prediction model of water inflow into drill and blast tunnels among several machine learning techniques. Autom Constr 127:103719. https://doi.org/10.1016/j.autcon.2021.103719

McJannet DL, Cook FJ, Burn S (2013) Comparison of techniques for estimating evaporation from an irrigation water storage. Water Resource Res 49(3):1415–1428. https://doi.org/10.1002/wrcr.20125

Miao XX, Cui XM, Wang JA, Xu JL (2013) The height of fractured water-conducting zone in undermined rock strata. Eng Geol 120(1–4):32–39. https://doi.org/10.1016/j.enggeo.2011.03.009

Parise M, Qiriazi P, Sala S (2004) Natural and anthropogenic hazards in karst areas of Albania. Nat Hazards Earth Syst Sci 4:569–581. https://doi.org/10.5194/nhess-4-569-2004

Poulsen BA, Adhikary DP, Elmouttie MK, Wilkins A (2015) Convergence of synthetic rock mass modelling and the Hoek-Brown strength criterion. Int J Rock Mech Min Sci 80:171–180. https://doi.org/10.1016/j.ijrmms.2015.09.022

Rajesh R, Ravi V, Venkata RR (2014) Selection of risk mitigation strategy in electronic supply chains using grey theory and digraph-matrix approaches. International Journal of Production Research 53(1): 238–257. https://doi.org/10.1080/00207543. 2014.948579

Ren C, An N, Wang JZ, Li L, Hu B, Shang D (2014) Optimal parameters selection for BP neural network based on particle swarm optimization: a case study of wind speed forecasting. Knowl-Based Syst 56:226–239. https://doi.org/10.1016/jknosys.2013.11.015

Roy DK, Barzegar R, Quilty J, Adamowski J (2020) Using ensembles of adaptive neuro-fuzzy inference system and optimization algorithms to predict reference evapotranspiration in subtropical climatic zones. Jourmal Hydrology 591:125509. https://doi.org/10.1016/j.jhydrol.2020.125509

Shi C (2019) Prediction mine water inrush by set water corridor method and comparison method. IOP Conf Series: Earth Environ Sci 300(2):022099. https://doi.org/10.1088/1755-1315/300/2/022099

Singh RN, Atkins AS (1985) Application of idealised analytical techniques for prediction of mine water inflow. Min Sci Technol 2:131–138. https://doi.org/10.1016/S0167-9031(85)90346-9

Waele JD, Gutiérrez F, Parise M, Plan L (2011) Geomorphology and natural hazards in karst areas: a review. Geomorphology 134(1–2):1–8. https://doi.org/10.1016/j.geomorph.2011.08.001

Wei JB, Wang SM, Song SJ, Sun Q, Yang T (2022) Experimental study on the deformation and failure mechanism of overburden rock during coal mining using a comprehensive intelligent sensing method. J Rock Mech Geotech Eng 14(5):1626–1641. https://doi.org/10.1016/J.JRMGE.2022.07.016

Wu Q, Zhao DK, Wang Y, Shen JJ, Mu WP, Liu HL (2017) Method for assessing coal-floor water-inrush risk based on the variable-weight model and unascertained measure theory. Hydrogeol J 25(7):2089–2103. https://doi.org/10.1007/s10040-017-1614-0

Wu WD, Wang TC, Bai JB, Liu JH, Wang XY, Xu HY, Feng GR (2024) Failure characteristics and cooperative control strategies for gob-side entry driving near an advancing working face: a case study. Processes 12(7):1398. https://doi.org/10.3390/pr12071398

Yanli H, Jixiong Z, Baifu A, Qiang Z (2011) Overlying strata movement law in fully mechanized coal mining and backfilling longwall face by similar physical simulation. J Min Sci 47(5):618–627. https://link.springer.com/article/10.1134/S1062739147050108

Yao BH, Bai HB, Zhang BY (2012) Numerical simulation on the risk of roof water inrush in Wuyang Coal Mine. Int J Min Sci Technol 22(2):273–277. https://doi.org/10.1016/j.ijmst.2012.03.006

Zaidel J, Markham B, Bleiker D (2010) Simulating seepage into mine shafts and tunnels with MODFLOW. J China Univ Min Technol Ground Water 48(3):390–400. https://doi.org/10.1111/j.1745-6584.2009.00659.x

Zarei HR, Uromeihy A, Sharifzadeh M (2011) Evaluation of high local groundwater inflow to a rock tunnel by characterization of geological features. Tunnelling and Underground Space Technology 26(2): 364–373. https://doi.org/10.1016/j.tust. 2010.11.007

Zeng YF, Meng SH, Wu Q, Mei AS, Bu WY (2023) Ecological water security impact of large coal base development and its protection. J Hydrol 619:129319. https://doi.org/10.1016/j.jhydrol.2023.129319

Zhao TB, Guo WY, Tan YL, Lu CP, Wang CW (2018) Case histories of rock bursts under complicated geological conditions. Bull Eng Geol Environ 77(4):1529–1545. https://doi.org/10.1007/s10064-017-1014-7

Zhu QH, Feng MM, Mao XB (2008) Numerical analysis of water inrush from working-face floor during mining. J China Univ Min Technol 18(2):159–163. https://doi.org/10.1016/S1006-1266(08)60034-6